GLOBAL BIOGEOCHEMICAL CYCLES, VOL. 26, GB4010, doi:10.1029/2012GB004380, 2012

High-resolution estimates of net community production and air-sea CO_2 flux in the northeast Pacific

Deirdre Lockwood,[1] Paul D. Quay,[1] Maria T. Kavanaugh,[2] Lauren W. Juranek,[2,3,4] and Richard A. Feely[3,4]

Received 2 April 2012; revised 27 August 2012; accepted 17 September 2012; published 30 October 2012.

[1] Rates of net community production (*NCP*) and air-sea CO_2 flux in the Northeast Pacific subarctic, transition zone and subtropical regions (22°N–50°N, 145°W–152°W) were determined on a cruise in August–September 2008 by continuous measurement of surface values of the ratio of dissolved oxygen to argon (O_2/Ar) and the partial pressure of CO_2 (pCO_2). These estimates were compared with simultaneous measurements of sea surface temperature (SST), chlorophyll-a (*chl-a*), flow cytometry, and discrete surface nutrient concentrations. *NCP* and CO_2 influx were greatest in the subarctic (45°N–50°N, 25.8 ± 4.6 and 4.1 ± 0.9 mmol C m^{-2} d^{-1}) and northern transition zone (40°N–45°N, 17.1 ± 4.4 and 2.1 ± 0.5 mmol C m^{-2} d^{-1}), with mean *NCP* ~6–8× greater than mean CO_2 invasion (error estimates reflect 1 σ confidence intervals). Contrastingly, the southern transition zone (32°N–40°N) and subtropics (22°N–32°N) had lower mean *NCP* (5.4 ± 1.8 and 8.1 ± 2.1 mmol C m^{-2} d^{-1}, respectively) and mean CO_2 efflux (3.0 ± 0.5 and 0.1 ± 0.0 mmol C m^{-2} d^{-1}, respectively). In the subarctic and transition zone, *NCP* was highly correlated with surface *chl-a* and CO_2 influx, indicating strong coupling between the biological pump and CO_2 uptake. Meridional trends in our *NCP* estimates in the transition zone and subtropics were similar to those for integrated summertime *NCP* along the cruise track determined using an upper ocean climatological carbon budget.

Citation: Lockwood, D., P. D. Quay, M. T. Kavanaugh, L. W. Juranek, and R. A. Feely (2012), High-resolution estimates of net community production and air-sea CO_2 flux in the northeast Pacific, *Global Biogeochem. Cycles*, *26*, GB4010, doi:10.1029/2012GB004380.

1. Introduction

[2] Surface CO_2 measurements yield a mean global net ocean sink for atmospheric CO_2 of ~2 Pg C yr^{-1}, however there is large variation in oceanic CO_2 uptake and release in both space and time [*Takahashi et al.*, 2009] that is controlled by biological drawdown through primary productivity (*PP*) and export to the deep ocean (the biological pump), temperature-driven solubility of CO_2 (the solubility pump) and ocean circulation. The biological pump has been estimated to export organic carbon globally at 8–15 Pg C yr^{-1} [*Emerson and Hedges*, 2008], but these rates are poorly constrained and vary widely across ocean regions [*Boyd and Trull*, 2007; *Schlitzer*, 2000, 2004]. To predict the response of this sink to future changes in Earth's climate, we must understand how the biological and solubility pumps vary spatially, seasonally and interannually, and what factors determine this variability.

[3] A remarkable feature in the surface CO_2 of the North Pacific is the band of strong mean annual air-sea CO_2 uptake (2–9 mol C m^{-2} yr^{-1}) at ~30°N–45°N, roughly corresponding to the transition zone between the subtropical and subarctic gyres along the path of the Kuroshio current and extension [*Takahashi et al.*, 2009]. Two prominent basin-wide oceanographic features occupy this region: (1) the physically defined North Pacific transition zone (~30°N–45°N), a region of confluence and convergence bounded by temperature and salinity fronts [*Roden*, 1991], and (2) the transition zone chlorophyll front (TZCF), a biological hot spot defined by the 0.2 mg m^{-3} chlorophyll isopleth that seasonally migrates from 30°N–35°N in winter to 40°N–45°N in summer [*Polovina et al.*, 2001].

[4] Given the biological prominence of the TZCF and the enhanced *PP* found at similar convergent fronts [*Longhurst*, 2007; *Mann and Lazier*, 2006], one would expect that *PP* and carbon export contribute substantially to the strong CO_2

[1]School of Oceanography, University of Washington, Seattle, Washington, USA.
[2]College of Earth, Ocean, and Atmospheric Sciences, Oregon State University, Corvallis, Oregon, USA.
[3]Joint Institute for the Study of the Atmosphere and Ocean, University of Washington, Seattle, Washington, USA.
[4]Pacific Marine Environmental Laboratory, NOAA, Seattle, Washington, USA.

Corresponding author: D. Lockwood, School of Oceanography, University of Washington, Seattle, WA 98195, USA. (delockwood@gmail.com)

0886-6236/12/2012GB004380

Table 1. Upper Ocean NCP in NE Pacific Subarctic, Subtropics, and Transition Zone[a]

Station	Annual NCP (mol C m^{-2} yr^{-1})	Daily NCP (mmol C m^{-2} d^{-1})
	Subarctic	
OSP	**2.0 ± 0.3** 2.1,[b] 1.8,[c] 2.1,[d] 1.6,[e] 2.5[f]	**14 ± 5** 12,[b] 8,[c] 15,[d] 10,[e] 17,[f] 21[g]
Alaska Gyre (∼50°N–55°N)	3.1[h]	18[h]
Subarctic current (∼45°N–50°N)	2.6[h]	15,[h] 25.8 ± 4.6[i]
	Subtropics	
ALOHA	**2.7 ± 0.9** 2.7,[j] 1.7,[k] 4.3,[l] 2.4,[m] 2.7,[n] 2.3[o]	**8 ± 4** 7,[j] 5,[k] 12,[l] 3,[m] 7,[n] 6,[o] 15[p]
20°N–25°N	2.4[q]	
145°W–152°W, 22°N–32°N		8.1 ± 2.1[i]
	Transition Zone	
All		**9 ± 5** (8; 3),[r] (21; 13),[s] 11.8 ± 3.2[i]
Northern (40°N–45°N)	2.6[t]	15,[t] 17.1 ± 4.4[i]
Southern (32°N–40°N)	0.9[t]	14,[t] 5.4 ± 1.8[i]

[a]See footnotes for seasonality of daily estimates. Values set in bold type are mean ± s.d. of previous observations cited below.
[b]*Wong et al.* [2002a], NO_3 mixed layer mass balance. Daily average over 6 months.
[c]*Charette et al.* [1999], ^{234}Th-^{238}U disequilibrium and Th/C ratio, mixed layer. August.
[d]*Emerson* [1987], O_2 mixed layer mass balance. Summer.
[e]*Emerson et al.* [1991], O_2, Ar and N_2 mixed layer mass balance. Summer.
[f]*Emerson and Stump* [2010], in situ O_2 and N_2 mixed layer mass balance. Summer.
[g]*Wheeler* [1993], 4-month NO_3 drawdown and $^{15}NO_3$ assimilation, mixed layer.
[h]*Wong et al.* [2002b]; NO_3 mixed layer mass balance. Daily average over summer NO_3 drawdown period.
[i]This study.
[j]*Emerson et al.* [1997], O_2 euphotic zone mass balance. Daily average over 12 months.
[k]*Hamme and Emerson* [2006], O_2 euphotic zone mass balance. Daily average over 12 months.
[l]*Emerson et al.* [2008], O_2 euphotic zone mass balance. Daily average over 12 months.
[m]*Benitez-Nelson et al.* [2001]; ^{234}Th deficiency over 0–150 m, includes total C output. August steady state POC export rate.
[n]*Quay and Stutsman* [2003], DIC-δ^{13}C mixed layer mass balance. Summer average.
[o]*Keeling et al.* [2004], δ^{13}C-DIC mixed layer mass balance. Daily average over 12 months.
[p]*Juranek and Quay* [2005], in situ mixed layer O_2/Ar. August.
[q]*Quay et al.* [2009], DIC-δ^{13}C mixed layer mass balance.
[r]*Howard et al.* [2010], euphotic zone O_2/Ar (summer, fall).
[s]*Juranek et al.* [2012], mixed layer O_2/Ar (spring, summer).
[t]*Wong et al.* [2002b]; NO_3 mixed layer mass balance. Daily average over summer NO_3 drawdown period.

uptake in this region, but the magnitude of this contribution is unclear. *Takahashi et al.* [2002, 2009] attribute the sink to the combined effects of the solubility and biological pumps. In contrast, *Ayers and Lozier* [2012] recently modeled CO_2 uptake in the transition zone and concluded that although temperature-driven solubility strongly affects seasonal pCO_2 trends, it controls only ∼17% of the annual sink in this region, with the remainder contributed by biological export and geostrophic divergence of DIC.

[5] In this study, we sought to estimate the contribution of the biological pump to carbon uptake in the North Pacific by making high-resolution estimates of carbon export and uptake. The strength of the biological pump is quantified by estimates of *NCP*, which equals gross *PP* (*GPP*) minus community respiration and is equivalent at steady state to the rate of organic carbon export and transfer up the food chain. In the North Pacific, *NCP* is fairly well constrained at two time series stations, Ocean Station P (OSP) in the subarctic NE Pacific (50°N, 145°W) and Station ALOHA in the subtropical NE Pacific (22°45N, 158°W) through surface layer budgets of dissolved gases, nutrients, *DIC* and $\delta^{13}C$, and through in situ dissolved gas ratios and ^{234}Th-^{238}U disequilibrium (see Table 1). But because there are comparatively fewer estimates in the rest of the basin and only a few snapshot *NCP* estimates for the transition zone [*Wong et al.*, 2002b; *Juranek*, 2007; *Howard et al.*, 2010; *Juranek et al.*, 2012], it is unclear how representative these sites are of the basin as a whole. On a basin-wide scale, *NCP* estimated from climatological seasonal *DIC* drawdown [*Lee*, 2001] is high (2–6 mol C m^{-2} yr^{-1}) in the transition zone.

[6] In recent years, fine-scale observations of oceanographic parameters made possible by continuous underway measurements have allowed researchers to better determine rates and controls on ocean biogeochemical processes, including *NCP*. In particular, continuous measurements of the dissolved gases O_2 and Ar using equilibrator inlet mass spectrometry (EIMS) [*Tortell*, 2005; *Kaiser et al.*, 2005; *Cassar et al.*, 2009], combined with a wind speed parameterization of gas exchange, have led to continuous, kilometer-scale estimates of *NCP* [e.g., *Nemcek et al.* 2008; *Guéguen and Tortell*, 2008; *Stanley et al.*, 2010; *Cassar et al.*, 2011].

[7] In this study, we continuously measured surface ocean O_2/Ar, pCO_2 and chl-a and carried out discrete flow cytometry in the subarctic, transition zone and subtropical Northeast Pacific to determine the heterogeneity in the rates of the biological pump and air-sea CO_2 *flux* on a cruise (August–September 2008) that crossed the transition zone three times (Figure 1). We compare these results with previous *NCP* estimates at OSP and Station ALOHA and surface CO_2 climatology, and examine the influence of *NCP* on CO_2 uptake in the region.

2. Background

2.1. Setting

[8] The main circulation features of the Northeast Pacific are the cyclonic subarctic gyre centered in the Gulf of Alaska

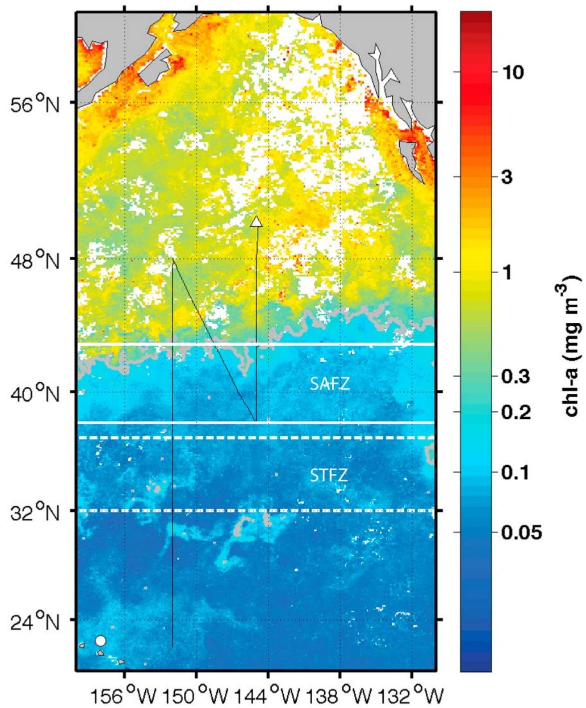

Figure 1. Cruise track (black) overlain on SeaWiFS 9-km monthly average *chl-a* for September 2008. White triangle, Station P; white circle, Station ALOHA. TZCF is highlighted in gray. Solid white lines bound SAFZ; dashed white lines bound STFZ.

(~45°N–60°N, 160°W–135°W), the anticyclonic subtropical gyre (~15°N–35°N, 135°E–135°W), and the transition zone between the two. In the subarctic Alaska gyre, a halocline limits winter mixed layer depths to ~90–120 m and strong seasonal variation in temperature and wind speed leads to stratification in summer, with mixed layers shoaling to ~40 m [*Harrison et al.*, 2004]. In this high nitrate, low chlorophyll (HNLC) region, iron generally limits the growth of large microphytoplankton like diatoms [*Harrison et al.*, 1999; *Boyd et al.*, 1996], and the phytoplankton community is dominated by small cells <5 μm.

[9] The subtropical gyre is a low-nutrient, low-chlorophyll region with lower seasonal variability in temperature, wind speed, productivity and light than in the subarctic gyre; mixed layer depth ranges from 40 m in summer to 100 m in winter [*Karl*, 1999; *Keeling et al.*, 2004]. *Prochlorococcus* is the dominant photoautotroph, but N_2 fixation by other cyanobacteria may provide up to half the nitrogen responsible for export [*Karl et al.*, 1997, 2001].

[10] Between these two gyres, the North Pacific transition zone extends across the basin at ~30°N–45°N. Confluence of the Kuroshio and Oyashio currents and Ekman convergence set up two frontal regions with strong meridional gradients in temperature and salinity in winter and salinity in summer, the subarctic frontal zone (SAFZ, defined by 33‰–33.8‰ isohalines, ~40°N–43°N) and the subtropical frontal zone (STFZ, defined by 34.8‰–35.2‰ isohalines, ~31°N–34°N [*Roden*, 1991]) (Figure 1). On shorter timescales, these frontal zones are associated with highly temporally and spatially variable mesoscale perturbations including meandering fronts, jets and eddies [*Roden*, 1991; *Yuan and Talley*, 1996].

2.2. Previous Estimates of *NCP* in the Northeast Pacific

[11] In the Northeast Pacific, most of our understanding of rates of net community productivity (*NCP*) comes from numerous studies at OSP in the subarctic gyre and Station ALOHA in the subtropical gyre, including mass balances of dissolved gases (O_2, Ar and N_2; *Emerson*, 1987; *Emerson et al.*, 1997, 1991; *Hamme and Emerson*, 2006; *Emerson and Stump*, 2010], NO_3 [*Wong et al.*, 2002a] and DIC-δ^{13}C [*Quay and Stutsman*, 2003; *Keeling et al.*, 2004; *Quay et al.*, 2009]; the in situ O_2/Ar method [*Juranek and Quay*, 2005; *Quay et al.*, 2010], and the ^{234}Th method [*Charette et al.*, 1999; *Benitez-Nelson et al.*, 2001].

[12] Notably, despite different limitations to biological productivity at these two sites, annual *NCP* is similar at 2.0 ± 0.3 mol C m^{-2} yr^{-1} at OSP and 2.7 ± 0.9 mol C m^{-2} yr^{-1} at ALOHA (mean ± s.d. of multiple estimates), within the ±50% uncertainty of the measurements (Table 1) [*Emerson et al.*, 2008]. However, at OSP, *NCP* is primarily confined to spring and summer at high daily rates (14 ± 5 mmol C m^{-2} d^{-1}), whereas at ALOHA, daily rates are lower (8 ± 4 mmol C m^{-2} d^{-1}) but *NCP* takes place throughout the year (mean ± s.d. of multiple studies, Table 1).

[13] Few studies have examined *NCP* in the transition zone. *Wong et al.* [2002b] estimated *NCP* at 2.6 mol C m^{-2} yr^{-1} and 0.9 mol C m^{-2} yr^{-1} based on seasonal NO_3 drawdown in two regions (40°N–45°N and 35°N–40°N, respectively). Summertime daily *NCP* for these two provinces was equal at 14–15 mmol C m^{-2} d^{-1}, but the southern region had a much shorter export season. *Juranek* [2007] and *Juranek et al.* [2012] estimated daily *NCP* in the transition zone mixed layer (~32°N–42°N) of 21 and 13 mmol C m^{-2} d^{-1} in spring and summer, respectively, and *Howard et al.* [2010] (30°N–45°N) estimated rates of 8 mmol C m^{-2} d^{-1} in summer and 3 mmol C m^{-2} d^{-1} in fall, based on O_2/Ar measurements (Table 1).

2.3. O_2/Ar Method for Estimating *NCP*

[14] The saturation level of the O_2/Ar gas ratio in the mixed layer coupled with air-sea gas exchange rate yields quantitative estimates of *NCP* that are mostly insensitive to nonbiological gas saturation processes (e.g., warming, bubble injection) because argon is an inert analog of oxygen, as described previously [*Craig and Hayward*, 1987 and *Emerson et al.*, 1991, 1997].

[15] Briefly, the biological O_2 supersaturation, which quantifies the influence of *NCP* on the O_2 budget, is defined as:

$$\frac{\Delta O_2}{Ar} = \frac{\left[\frac{O_2}{Ar}\right]_{msr}}{\left[\frac{O_2}{Ar}\right]_{sat}} - 1 \tag{1}$$

where $[O_2/Ar]_{msr}$ is the measured dissolved O_2/Ar gas ratio, and $[O_2/Ar]_{sat}$ is the ratio expected at saturation with air (based on temperature and salinity dependence of O_2 and Ar solubility [*García and Gordon*, 1992; *Hamme and Emerson*, 2004]). The percent biological O_2 supersaturation ($\%O_{2bio}$) equals ($\Delta O_2/Ar$)*100.

[16] *NCP* is calculated using O_2 and Ar mass balances for the mixed layer, typically assuming steady state and negligible physical supply, yielding:

$$NCP = k_{O2}[O_2]_{sat}\frac{\Delta O_2}{Ar} \quad (2)$$

where k_{O2} is the gas transfer velocity of O_2 (m d^{-1}) and $[O_2]_{sat}$ is the concentration of O_2 at saturation (mol m^{-3}) [*García and Gordon*, 1992]. We determined k_{O2} using winds from QuikScat, the *Ho et al.* [2006] wind speed parameterization using a 60-day time-weighting technique [*Reuer et al.*, 2007], and the temperature- and salinity-dependent Schmidt number [*Wanninkhof*, 1992]. To convert O_2-based *NCP* to C-based *NCP*, we used a ratio of 1.4 O_2: 1 C (export or new production) [*Laws*, 1991]. This estimate of *NCP* integrates over the residence time of O_2 in the mixed layer (i.e., (mixed layer depth)/k_{O2}), which was 8–14 days. The strong vertical stratification and low winds observed during the cruise favored a negligible impact of vertical mixing on the mixed layer O_2 budget.

3. Methods

3.1. Underway and Discrete Sampling and Cruise Track

[17] We continuously measured surface O_2/Ar, pCO_2, temperature, salinity and fluorescence from the underway system of the R/V Thompson (at ~5 m intake) on a cruise betwen Station P and Honolulu, Hawaii (30 August–15 September 2008; Figure 1). Temperature and salinity were measured using the ship's TSG. Underway chl-a was estimated based on continuous fluorometer measurements calibrated with discrete chl-a samples measured using standard methods on a shipboard Turner fluorometer [*Strickland and Parsons*, 1972]. Mixed layer depth was determined using CTD profiles along the ship's cruise track at a resolution of ~1°–2° latitude as a density increase of 0.125 kg m^{-3} from the surface value. Concentrations of nitrate, phosphate and silicate were determined on discrete surface samples collected by Niskin using a shipboard autoanalyzer (Technicon AutoAnalyzer II) and standard methods [*Intergovernmental Oceanography Commission*, 1994].

3.2. Continuous O_2/Ar Measurements Using EIMS

[18] We continuously measured surface O_2/Ar using an EIMS system similar to that described in *Cassar et al.* [2009]. Water from the ship's underway line was pumped at ~2 L min^{-1} through a coarse filter to screen out particulates into a 1 L graduated cylinder on which the equilibrator cartridge (Membrana MicroModule G569, 0.75″ × 1″) was mounted. Water from the graduated cylinder was pumped through a 5 μm filter sock sewed inside a 100 μm filter sock (1.5″ × 12″, McMaster-Carr), and then through the cartridge at ~100 ml min^{-1}. To prevent biofouling, the coarse filter was cleaned and the sock filter was replaced daily, and the equilibrator cartridge was replaced weekly. All tubing used was Tygon silver (antimicrobial).

[19] Headspace gas from the equilibrator was delivered through an 0.05 mm fused silica capillary to the quadrupole mass spectrometer (Pfeiffer Prisma QMS), which was kept at a constant temperature (40° ± 2°C). Individual ion currents (O_2, Ar) were measured at 1-s intervals, and the ratio of O_2/Ar currents was averaged to a 10-min timescale. The EIMS system e-folding response time is 7 min [*Cassar et al.*, 2009], yielding a spatial resolution of ~2 km at the average ship speed of 10 knots.

[20] EIMS-based O_2/Ar measurements were calibrated using the O_2/Ar of air measured by the EIMS, and O_2/Ar measured by isotope ratio mass spectrometer (IR-MS) on discrete samples collected from either the underway line or surface (5 m) Niskin bottles approximately every 6–8 h following the collection procedures of *Emerson et al.* [1995] and mass spectrometer procedures of *Juranek and Quay* [2005] in the University of Washington Stable Isotope Lab. The percent error ([s.d./mean]*100) in O_2/Ar of discrete air standards used for IR-MS calibration was 0.2% and that of duplicate samples was 0.1%. The O_2/Ar of discrete samples measured simultaneously on the ship's underway line and from surface Niskins compared well (0.1% error), showing no evidence of O_2 consumption in the underway line.

[21] We estimated error in *NCP* using a Monte-Carlo approach assigning uncertainty in the following terms: kO_2 ± 15% (twice the spread in k_{O2} values predicted by three parameterizations recently validated by *Ho et al.* [2011]: *Nightingale et al.* [2000], *Ho et al.* [2006], and *Sweeney et al.* [2007]) and O_2/Ar ± 0.06 (s.d. of mean in offset between EIMS and discrete samples). Mean *NCP* percentage error ([s.d./mean]*100) was 18% in the subarctic, 27% in the transition zone and 25% in the subtropics.

3.3. Measurements of pCO_2 and Estimate of CO_2 Flux

[22] We continuously measured the pCO_2 in surface water from the ship's underway line and air from the bow with an automated IR-detection-based underway pCO_2 measuring system that has been described in detail elsewhere [*Feely et al.*, 1998; *Pierrot et al.*, 2009]. We calculated the air-sea pCO_2 gradient (ΔpCO_2) as $\Delta pCO_2 = pCO_{2SW} - pCO_{2atm}$, where pCO_{2SW} is the calculated pCO_2 of the seawater (after correction for water temperature difference between in situ and the pCO_2 equilibrator) and pCO_{2atm} is the measured atmospheric pCO_2. After correction, the accuracy of the data is within 0.1 μatm for pCO_{2atm} and 2 μatm for pCO_{2SW} [*Pierrot et al.*, 2009], and the equilibrator integration time is 30–45 s. pCO_2 data were averaged to match the 10-min integration time of the EIMS data.

[23] The air-sea flux of CO_2 is calculated based on ΔpCO_2 and the solubility (k_H) [*Stumm and Morgan*, 1996] and gas transfer velocity of CO_2 (k_{CO2}):

$$CO_2flux = k_{CO2}k_H\Delta pCO_2 \quad (3)$$

Defined in this way, *CO_2 flux* from the atmosphere into the ocean (influx) is negative, and efflux is positive. k_{CO2} was calculated as described above for k_{O2} using the *Ho et al.* [2006] wind speed parameterization with time-weighting [*Reuer et al.*, 2007], and the Schmidt number for CO_2 [*Wanninkhof*, 1992].

3.4. Flow Cytometry Measurements

[24] Cell counts of phytoplankton groups were collected from the flow-through system of the R/V Thompson at

various intervals along the ship track or from surface (5 m) Niskins. Samples were preserved in liquid nitrogen and processed later in the lab. Cells were enumerated and classified using a FACS-Caliber flow cytometer [*Sherr et al.*, 2005]. Following the protocol of *Sherr et al.* [2005], prokaryotes were stained with SYBR-green; *Prochlorococcus* counts were subtracted from heterotrophic bacteria counts. We binned data into microphytoplankton (10–60 μm), nanophytoplankton (2–10 μm) and picophytoplankton (1–2 μm); the picophytoplankton fraction was dominated by *Synechococcus* north of the TZCF and *Prochlorococcus* south of it.

3.5. Climatological pCO_2, CO_2 Flux, Alkalinity and DIC

[25] We used a recent climatological surface pCO_2 data set [*Takahashi et al.*, 2009] to compare our pCO_2 measurements with the seasonal cycle of pCO_2 and DIC over our cruise track (section 5.3). This data set includes monthly pCO_{2SW}, pCO_{2atm}, SST, salinity and wind speed data at resolution of 4° latitude × 5° longitude, with pCO_2 data normalized to reference year 2000. We calculated climatological monthly *CO_2 flux* using the climatological pCO_{2SW}, pCO_{2atm}, temperature, salinity, wind speed and *Ho et al.* [2006] parameterization of gas transfer velocity and compared it to our continuous *CO_2 flux* estimates in September 2008 (normalized to year 2000).

[26] To estimate the seasonal climatological *DIC* cycle for the region covered on our cruise, we used the climatological temperature and salinity data to calculate monthly alkalinity with the latitude-dependent parameterization of *Lee et al.* [2006], and used these alkalinity values and pCO_2 to calculate monthly *DIC* with the program CO2sys [*Lewis and Wallace*, 1998]. We used monthly climatological mixed layer depth from *Monterey and Levitus* [1997] at 1° resolution, bin-averaged to the 4° latitude × 5° longitude boxes of the *Takahashi et al.* [2009] data set.

4. Results

4.1. Regional Setting

[27] We categorize our results into three regions: the subarctic (45°N–50°N), transition zone (32°N–45°N) and subtropics (22°N–32°N). Sea surface temperature and salinity generally increased and density decreased from the subarctic to the subtropical gyre, with a local density minimum at ~35°N within the transition zone (Figure 2). The strong gradients in surface salinity (and weaker SST gradients) of the SAFZ and STFZ are apparent (Figure 2) at ~38°N–43°N, and ~32°N–37°N, respectively, extending slightly farther than their climatological positions (40°N–43°N and 31°N–34°N, respectively). The strongest surface density gradients were in the northern transition zone (40°N–45°N) and subtropics (22°N–24°N) (Figure 2). The TZCF (location of the 0.2 mg m^{-3} chl-a isopleth) ranged from 42°N to 44°N within the northern transition zone (Figure 3), consistent with its climatological late summer position (40°N–45°N) [*Polovina et al.*, 2001].

[28] Mixed layer was relatively shallow, reflecting late summer conditions; mean depths decreased from 32 m in the subarctic to a local minimum (26 m) in the transition zone, and then increased to 51 m in the subtropics (Figure 2). k_{O2} was fairly low (3–5 m d^{-1}), and was highest in the subarctic and northern transition and lowest in the southern transition zone (Figure 3). Due to variation in mixed layer depth and k_{O2}, the O_2 residence time in the surface layer increased southward from a mean of 8 days in the subarctic and transition to 14 days in the subtropics.

4.2. Subarctic

[29] In the subarctic, we observed high biological O_2 saturation (*$\%O_{2bio}$*) and *chl-a* and low ΔpCO_2, with high meridional and zonal variability (Figure 3). *$\%O_{2bio}$* and *chl-a* were highly correlated. pCO_2 was highly negatively correlated with *$\%O_{2bio}$* and *chl-a*, and only weakly correlated with SST (Table 2). At the southern edge of the subarctic along 145°W, strong peaks in *$\%O_{2bio}$* and *chl-a* were coupled with troughs in ΔpCO_2 (Figure 3). Surface nutrient concentrations at OSP (6 μM nitrate and 4 μM silicate, respectively) were lower than typical late summer concentrations of 9 μM nitrate and 14 μM silicate [*Harrison et al.*, 2004] (Figure 3).

[30] *NCP* and CO_2 influx had similar spatial trends to *$\%O_{2bio}$* and ΔpCO_2, and their mean values were highest in the subarctic among cruise regions (25.8 mmol C m^{-2} d^{-1} and 4.1 mmol C m^{-2} d^{-1}, respectively; Figure 4). *NCP* was highly correlated with CO_2 influx (r = 0.89), with a slope of 2.6 (Table 2). Flow cytometry results (Figure 4) show high concentrations of all three phytoplankton classes in the subarctic. *NCP* was most highly correlated with concentrations of microphytoplankton (r = 0.50) in this region.

4.3. Transition Zone

[31] The transition zone represented a shift from the high-chl-a, high-*$\%O_{2bio}$*, low-pCO_2, high-nutrient conditions of the subarctic to opposite conditions in the subtropics. At the boundary between the northern transition zone and subarctic, in the vicinity of the TZCF, we observed coincident peaks in *$\%O_{2bio}$* and *chl-a* and troughs in ΔpCO_2, with high zonal variability (Figure 3). In the southern transition zone (32°N–40°N), *$\%O_{2bio}$* and chl-a decreased. At ~42°N, pCO_2 shifted from undersaturated values to the north to supersaturated values to the south, and remained supersaturated in the southern transition zone.

[32] Throughout the transition zone, *chl-a* and *$\%O_{2bio}$* were positively correlated (r = 0.85), and pCO_2 and *$\%O_{2bio}$* were negatively correlated (r = −0.75), similarly to the subarctic. But in contrast with the subarctic, pCO_2 was positively correlated with SST (r = 0.87; Table 2). Surface nitrate and silicate declined from the subarctic to northern transition zone; nitrate approached the detection limit at the TZCF and remained <1 μM in the southern transition zone.

[33] From the northern to the southern transition zone, *NCP* declined (mean 17.1 and 5.4 mmol C m^{-2} d^{-1}, respectively), and *CO_2 flux* varied from an influx to an efflux (Figure 4 and Table 2). Meridional and zonal (145°W–152°W) variability in fluxes were high in the northern transition zone. Throughout the transition zone, *NCP* and CO_2 influx were correlated with a similar r (0.85) and slope (2.4) to that in the subarctic (Table 2).

[34] Throughout the transition zone, *NCP* was highly correlated with microphytoplankton and nanoplankton (r = 0.89 and 0.83, respectively), and less strongly correlated with picophytoplankton (r = 0.58). NCP was also highly correlated with the fraction of total cell count made up by

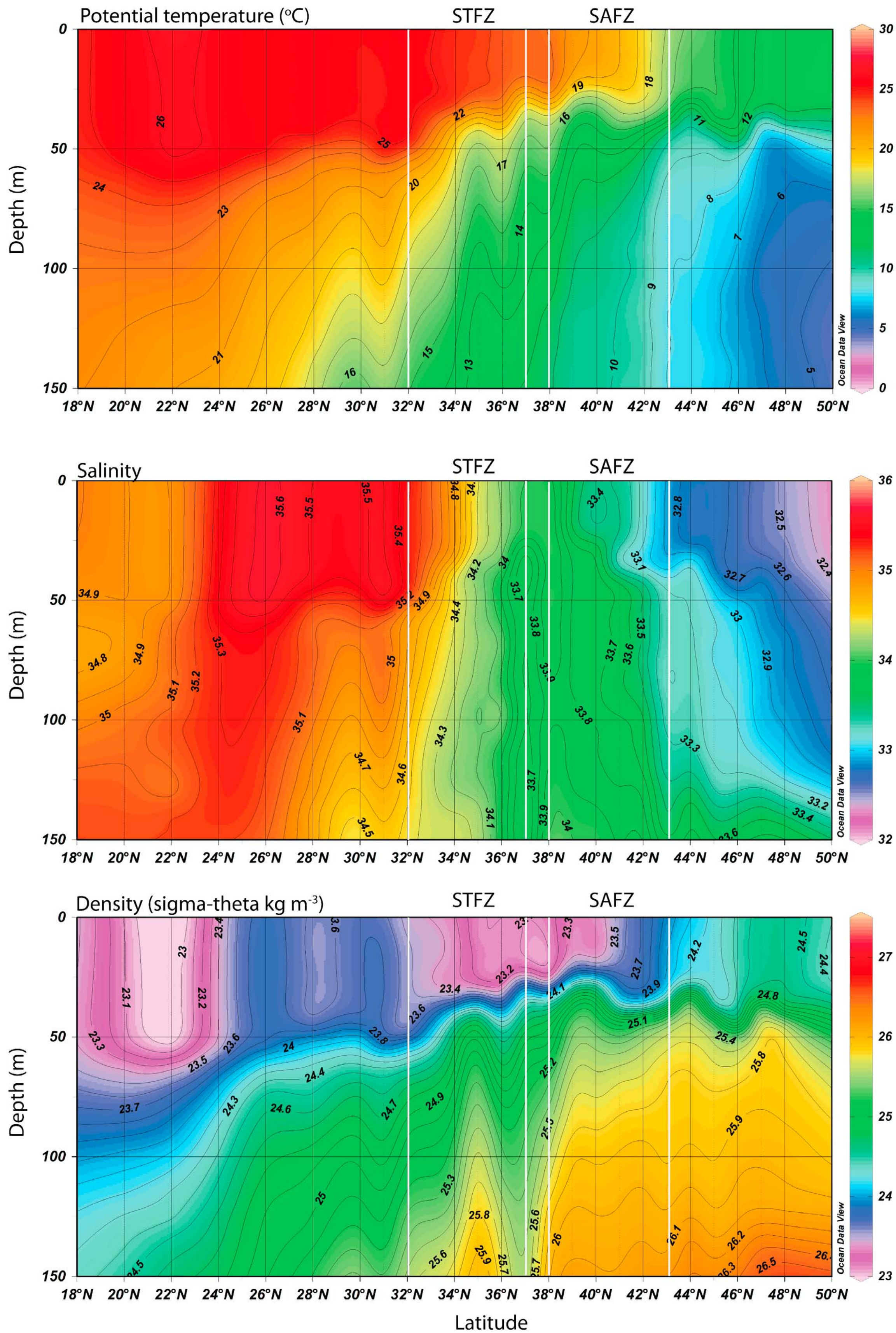

Figure 2. Depth sections of potential temperature, salinity and potential density (σ_θ) measured on cruise along 152°W. The SAFZ and STFZ are bounded with white lines.

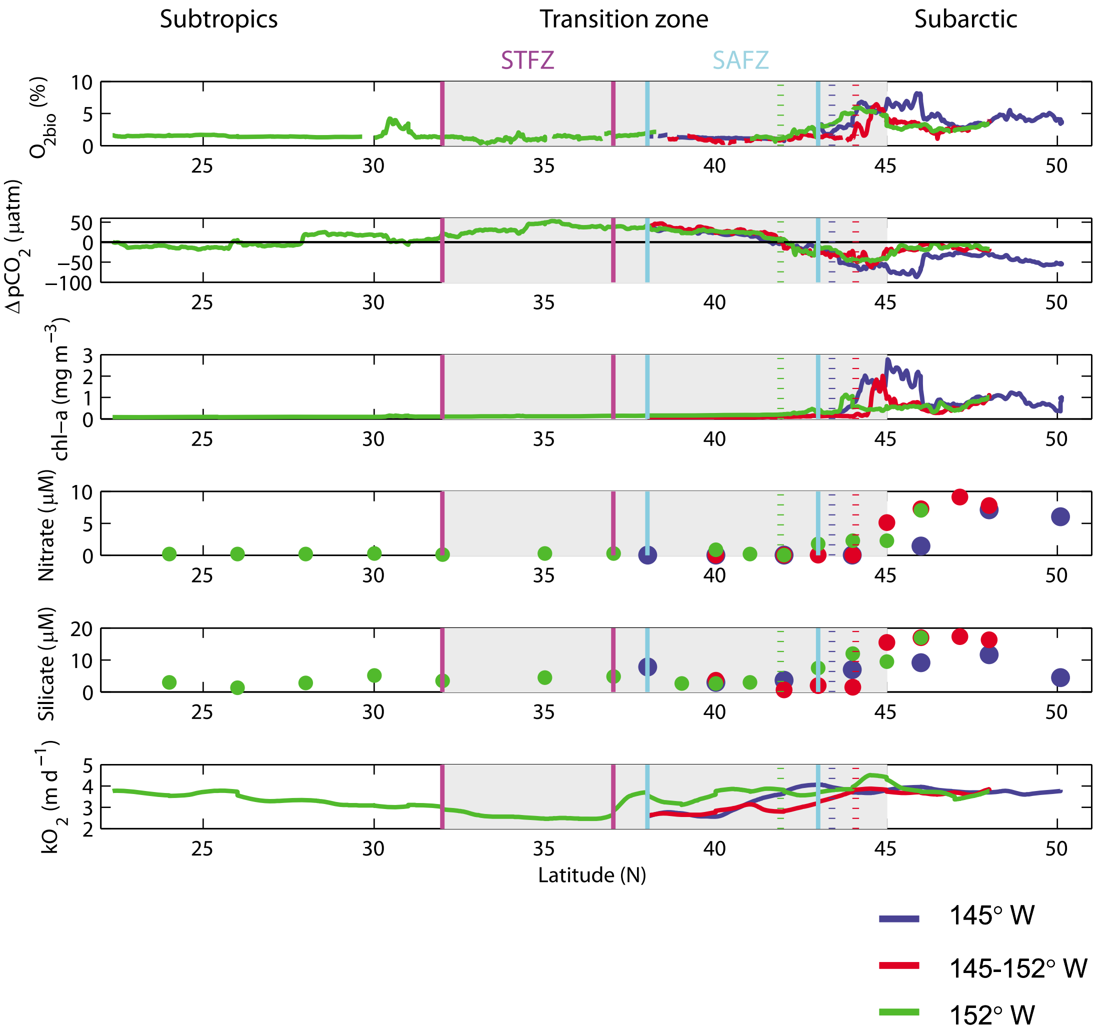

Figure 3. Continuous underway measurements of surface %O_{2bio}, $\Delta p\mathrm{CO_2}$, *chl-a*, nitrate, silicate and k_{O2} along three legs of cruise track. Blue and magenta lines bound SAFZ and STFZ, respectively. Dotted vertical lines, position of TZCF (colors refer to cruise legs; see key). Transition zone is highlighted in gray.

microphytoplankton (r = 0.72). In the northern transition zone, high abundance of micro- and nanophytoplankton coincided with high *NCP* and CO_2 uptake (Figure 4).

4.4. Subtropics

[35] In the subtropics, %O_{2bio}, chl-a, and nutrients were low, similar to conditions in the southern transition zone, with the exception of a small peak in %O_{2bio} at 30.5°N. $\Delta p\mathrm{CO_2}$ generally decreased southward from a maximum in the southern transition zone. Throughout the subtropics, chl-a was highly correlated with %O_{2bio} (r = 0.86). $p\mathrm{CO_2}$ was weakly negatively correlated with both %O_{2bio} and SST (Table 2). Surface nitrate was below detection limit throughout most of the subtropics, and surface silicate averaged 3 μM.

[36] Mean *NCP* in the subtropics (8.1 mmol C m^{-2} d^{-1}; Figure 4) was slightly higher than that in the southern transition zone. Mean *CO_2 flux* was close to zero, and CO_2 influx was weakly correlated with *NCP* (Figure 4 and Table 2). *NCP* was weakly correlated with picophytoplankton (*Prochlorococcus*) throughout the subtropics (Table 2). A peak in *NCP* at ~30.5°N of 22 mmol C m^{-2} d^{-1} corresponded to a small CO_2 influx. In the region of this peak (30°N–31.2°N), *NCP* was highly correlated with *chl-a* (r = 0.97) and CO_2 influx (r = 0.69), and the *NCP*:CO_2 influx slope (3.3) was similar to that observed in the subarctic and northern transition zone (Table 2).

5. Discussion

5.1. Rates of *NCP* and CO_2 Uptake

[37] In the subarctic, *NCP* (25.8 ± 4.6 mmol C m^{-2} d^{-1}) and CO_2 influx (4.1 ± 0.9 mmol C m^2 m^{-2} d^{-1}) reached their highest mean values along the cruise track. These values were ~2× higher than the mean of previous estimates of *NCP* and climatological CO_2 influx for this region (Table 1 and *Takahashi et al.* [2009, Table 2]). Mean *chl-a* (0.8 mg m^{-3}) was almost twice as high as usual for September based on the SeaWiFS 9-km *chl-a* time series for 1997–2010 (Figure 5), reflecting a phytoplankton bloom in this region. This bloom was most likely stimulated by iron deposited with volcanic ash in the early August 2008 eruption of the Aleutian island volcano Kasatochi [*Hamme et al.*, 2010; *Langmann et al.*, 2010].

Table 2. Mean Values and Correlation Statistics for Underway Measurements

Region	NCP[a] (mmol C m^{-2} d^{-1})	CO_2 $flux$[a] (mmol C m^{-2} d^{-1})	Climatol. CO_2 $flux$[b] (mmol C m^{-2} d^{-1})	Chl-a (μg m^{-3})	Correlation Coefficient (r): %O_{2bio}-chl-a	%O_{2bio}-pCO$_2$	SST-pCO$_2$	NCP-CO$_2$ Influx	SST-CO_2 $flux$	NCP-micro / NCP-f_{micro}	NCP-nano / NCP-f_{nano}	NCP-pico / NCP-f_{pico}	Slope NCP-CO$_2$ Influx
Subarctic	25.8 ± 4.6 [9.3]	−4.1 ± 0.9 [3.1]	−1.7 ± 0.3	0.8	0.82	−0.81	0.10	0.89	−0.17	0.50	0.17	0.15	2.8
(45°N–50°N)										0.18	−0.08	0.05	
Transition	11.8 ± 3.2 [11.8]	0.2 ± 0.0 [4.0]	1.5 ± 1.3	0.3	0.85	−0.75	0.87	0.85	0.84	0.89	0.83	0.58	2.4
(32°N–45°N)										0.73	0.07	−0.16	
Northern	17.1 ± 4.4 [13.7]	−2.1 ± 0.5 [4.0]	1.1 ± 1.0	0.4	0.83	−0.78	0.94	0.84	0.95	0.86	0.73	0.37	2.9
(40°N–45°N)										0.75	0.05	−0.14	
Southern	5.4 ± 1.8 [2.3]	3.0 ± 0.5 [0.7]	2.6 ± 1.8	0.1	0.54	0.21	0.18	−0.57	0.08*	0.68	0.21	−0.32	−1.6
(32°N–40°N)										0.40	0.31	−0.33	
Subtropics													
(22°N–32°N)													
All data	8.1 ± 2.1 [2.6]	0.1 ± 0.0 [1.3]	0.8 ± 0.1	0.1	0.86	−0.17	−0.50	0.34	−0.50	0.12	−0.21	0.32	0.7
										0.08	−0.28	0.19	
Bloom region	12.3	0.5	–	0.1	0.97	−0.69	−0.79	0.71	−0.79	0.74	−0.26	0.50	3.3
(30°N–31.2°N)										−0.11	−0.57	0.52	

[a]Values for NCP and CO_2 $flux$ are mean ± error of 1 σ (regional s.d. is in brackets). Negative CO_2 $flux$ represents oceanic CO$_2$ uptake. Correlation coefficient (r) is shown between two parameters listed at top of each column. All correlations were significant ($P < 0.001$ for all cells except cell marked with an asterisk, $P < 0.02$). Micro, microphytoplankton; nano, nanophytoplankton; pico, picophytoplankton; f_{micro}, f_{nano} and f_{pico} are the respective fractions of total cell count made up by these phytoplankton classes.

[b]Climatological CO_2 $flux$ is presented for comparison, aligned with climatological boxes that most closely correspond to it: subarctic, 46°N–50°N; transition, 30°N–46°N; northern transition, 38°N–46°N; southern transition, 30°N–38°N; subtropics, 22°N–30°N.

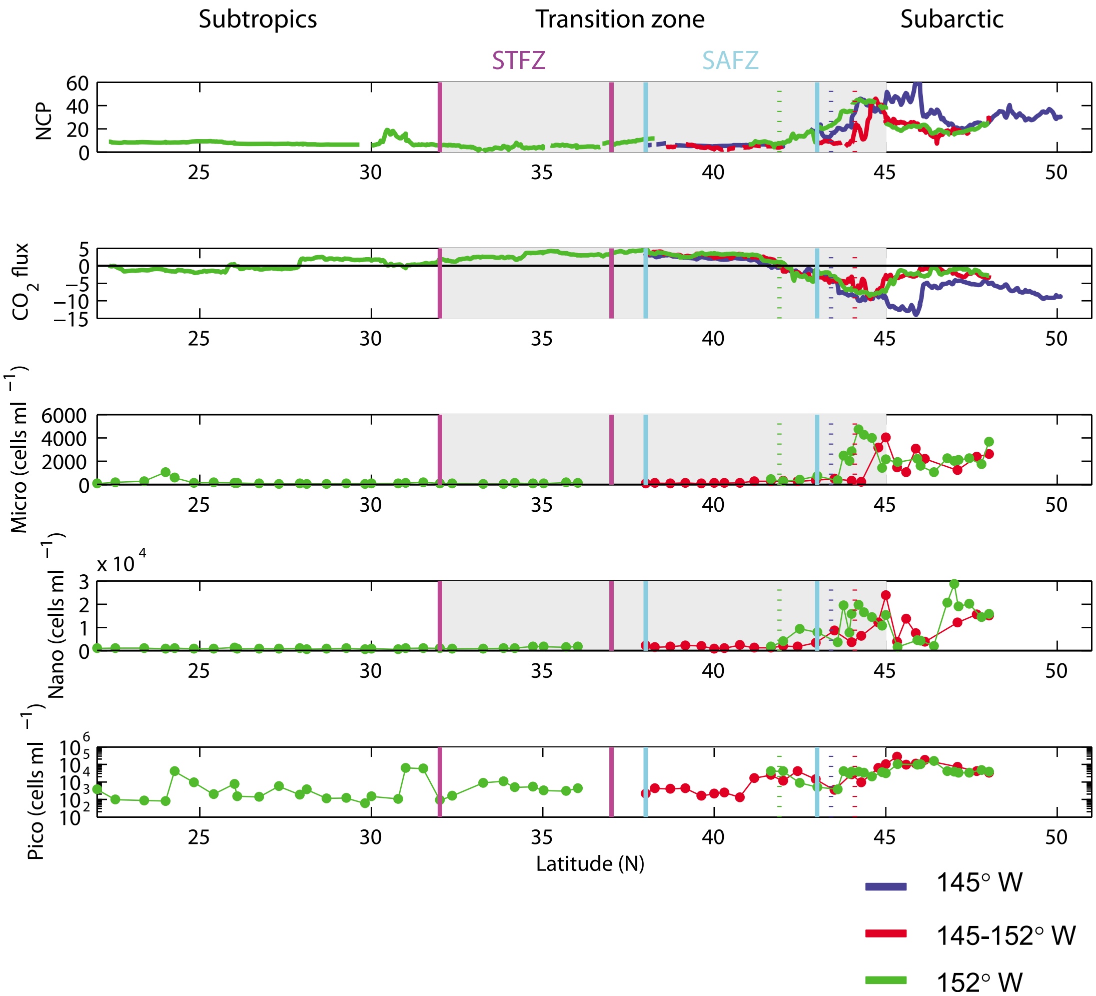

Figure 4. Continuous estimates of *NCP* and *CO_2 flux* and flow cytometry-derived concentrations of microphytoplankton (10–60 μm), nanophytoplankton (2–10 μm) and picophytoplankton (1–2 μm) along legs of cruise track. Units of *NCP* and *CO_2 flux* are mmol C m^{-2} d^{-1}; negative *CO_2 flux* represents oceanic CO_2 uptake. Picophytoplankton represent *Synechococcus* north of the TZCF and *Prochlorococcus* south of it. Blue and magenta lines bound SAFZ and STFZ, respectively. Dotted vertical lines, position of TZCF (colors refer to cruise legs; see key). Transition zone is highlighted in gray.

[38] The high *NCP* and CO_2 influx in the subarctic estimated during our cruise were consistent with bloom conditions, although there is evidence that we sampled during a declining stage of this bloom. SeaWiFS *chl-a* in our cruise region declined from August to September and onward (Figure 5). At OSP, our O_2/Ar-based *NCP* on 30 August (30 mmol C m^{-2} d^{-1}) was lower than O_2/Ar-based *NCP* (43 mmol C m^{-2} d^{-1}) estimated on 21 August [*Hamme et al.*, 2010].

[39] In the subtropics, mean *NCP* (8.1 ± 2.1 mmol C m^{-2} d^{-1}) was very similar to that previously observed at ALOHA (8 ± 4 mmol C m^{-2} d^{-1}; Table 1), indicating that observations at this station are generally representative of the NE Pacific subtropical region. *CO_2 flux* showed a weak efflux (0.1 ± 0.0 mmol C m^{-2} d^{-1}), ~8× lower than climatological September CO_2 efflux (Table 2). *Chl-a* in the subtropics (0.1 mg m^{-3}) was similar to typical September values from the SeaWiFS time series (Figure 5).

[40] Although *NCP* in the subtropics was ~3× lower than in the subarctic during our cruise, we observed a peak in *NCP* at 30°N–31°N, 152°W (Figure 4) associated with the late summer bloom that has been previously observed in this region (~30°N, 130°W–160°W) and that can last up to 3–4 months [*Wilson et al.*, 2008]. This recurrent bloom has been attributed both to N_2 fixation by unicellular cyanobacteria and endosymbionts, and to *Rhizosolenia* diatom mats that can vertically migrate into the nitracline through ballasting [*Wilson*, 2003; *Wilson et al.*, 2008]. *NCP* estimates at 30°N–31°N peaked at 19 mmol C m^{-2} d^{-1}, approximately twice the mean subtropical rate.

[41] The transition zone (32°N–45°N) had mean *NCP* intermediate between the subarctic and subtropics (11.8 ± 3.2 mmol C m^{-2} d^{-1}; Table 2), and within the range of previous *NCP* estimates in both the subarctic and transition zone (Table 1). Notably, *NCP* in the transition zone had much higher spatial variability than in the subarctic or subtropics, with regional s.d. of 11.8, equivalent to the mean (Table 2). It had mean CO_2 efflux (0.2 ± 0.0 mmol C m^{-2} d^{-1}) that was ~7× lower than September climatological efflux (Table 2).

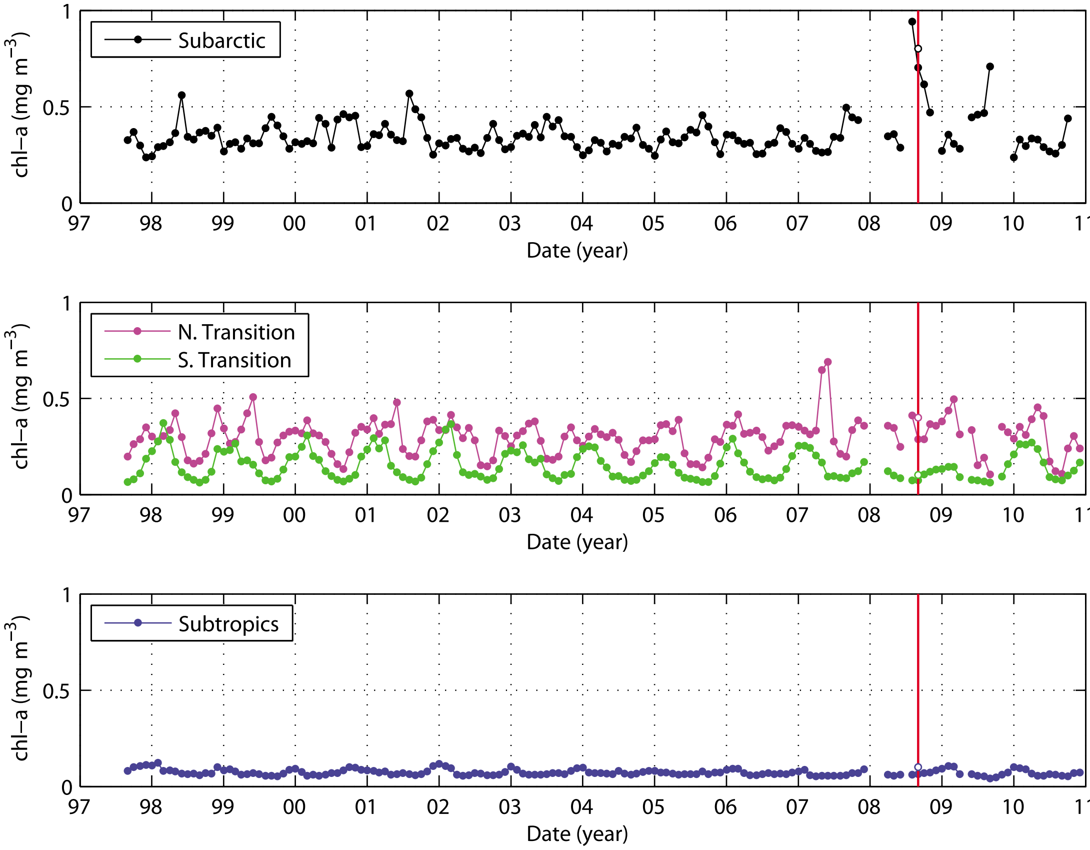

Figure 5. Time series of monthly satellite-based SeaWiFS 9-km *chl-a* (1997–2010) averaged over cruise regions (longitude 145°W–155°W, latitudes 45°N–50°N for subarctic, 40°N–45°N for northern transition, 32°N–40°N for southern transition, 22°N–30°N for subtropics). Grid lines mark beginning of each year. Red line marks month of cruise and open circles show mean *chl-a* measured on cruise. Figure made using data from NASA Giovanni.

[42] In the northern transition zone, mean *NCP* (17.1 ± 4.4 mmol C m^{-2} d^{-1}) was similar to a previous estimate in this region (Table 1) and on the high end of previous summertime *NCP* estimates in the subarctic. Both meridional and zonal (145°W–152°W) *NCP* variability were high in this region (regional s.d. = 13.7, Table 2). CO_2 influx (2.1 ± 0.5 mmol C m^{-2} d^{-1}) here was greater than climatological September estimates, which show a mean efflux of 1.1 ± 1.0 mmol C m^{-2} d^{-1} (Table 2); this discrepancy could be attributable to the anomalous bloom conditions in the subarctic, or to interannual variability in the frontal dynamics of the transition region. Based on the SeaWiFS time series (Figure 5) *chl-a* was not anomalously high during our cruise in either of these regions, as it was in the subarctic. In the southern transition zone, *NCP* at 5.4 ± 1.8 mmol C m^{-2} d^{-1} was similar to previous estimates at ALOHA, and mean CO_2 efflux was 3.0 ± 0.5 mmol C m^{-2} d^{-1}, similar to the September climatological value in this region (Table 2).

[43] Compared with a wealth of *NCP* estimates at OSP in the subarctic and ALOHA in the subtropics, we have only a few snapshots of *NCP* in the transition zone. Based on our results and previous studies, *NCP* in the northern transition zone resembles the subarctic, with comparably high summertime daily *NCP* rates (Table 1) and a strong link between *NCP* and CO_2 uptake. We observed the highest spatial variability in *NCP* and *CO_2 flux* in this region, and it has high interannual variability in satellite *chl-a* (Figure 5). Frontal dynamics in this region likely play a role in this temporal and spatial biological patchiness, as we discuss further below. In contrast, the southern transition zone resembles the subtropical gyre, with lower daily *NCP* rates that peak in spring, lower spatial variability and a summertime CO_2 efflux.

5.2. Impact of *NCP* on CO_2 Uptake

[44] Through the high spatial resolution of our measurements, we observed several regions in which *NCP* and CO_2 influx were highly coupled, demonstrating a link between the biological pump and atmospheric CO_2 uptake on a ~2-week timescale. In the subarctic, we observed this high correlation during the decline of the anomalous bloom (including micro- and nanophytoplankton) described above, most likely stimulated by volcanic deposition of iron. This could be characteristic of the "event-driven, mass sedimentation carbon pump" described by *Karl et al.* [2003] in which perturbations such as pulsed delivery of iron lead to blooms and aggregation of large phytoplankton like diatoms, resulting in rapid, efficient export events. These

results indicate that intermittent iron supply in this region (through volcanic events, eddy transport from the continental shelf or atmospheric deposition) would lead to a stronger carbon sink on short-term (seasonal) timescales.

[45] Throughout the transition zone, we observed similarly high correlation between *NCP* and CO_2 influx. *NCP* was highly correlated with concentrations of micro- and nanoplankton, which were abundant in the northern transition zone, and was highly correlated with the fraction of total cell count comprising microphytoplankton. The SAFZ, STFZ and TZCF have been found to be associated with high *PP*, *NCP* and abundance of microphytoplankton by other researchers [*Leonard et al.*, 2001; *Juranek*, 2007; *Howard et al.*, 2010; *Juranek et al.*, 2012].

[46] Frontal dynamics may play a role in the biological patchiness observed in the transition zone due to (i) mesoscale perturbations associated with frontal zones, leading to dynamic upwelling [*Roden*, 1991; *Olson et al.*, 1994] that can bring nutrients to the surface and stimulate phytoplankton growth [*Strass*, 1992; *Denman and Gargett*, 1995]; (ii) variations in Ekman convergence and resulting nutrient supply at the TZCF [*Ayers and Lozier*, 2010]; and (iii) convergence of biomass (phytoplankton) at the TZCF [*Polovina et al.*, 2001], as has been observed at similar convergent fronts [*Mann and Lazier*, 2006; *Franks*, 1992; *Olson et al.*, 1994].

[47] In the subtropics, phytoplankton abundance (*chl-a*) and $\%O_{2bio}$ were highly correlated as in the subarctic (Figure 3), but there was a much lower correlation between *NCP* and CO_2 influx (Table 2; $r = 0.20$ versus $r = 0.89$ in the subarctic). This probably results from the strong influence of temperature on the summertime *CO_2 flux* in this region, yielding a weaker link between *NCP* and CO_2 uptake. The dominance of picophytoplankton over nano- and microphytoplankton in the subtropics (Figure 3) may also lead to less efficient export.

[48] We observed a peak in *NCP* at ~30°N, 130°W–160°W, where recurrent late summer phytoplankton blooms have been observed. In this region (30°N–31.2°N), *NCP* was highly correlated with *chl-a* and CO_2 influx, and the slope of this correlation was similar to that observed in the subarctic and transition zone (Table 2). At this location, microphytoplankton and picophytoplankton (*Prochlorococcus*) dominated, and their abundances were highly correlated with *NCP* ($r = 0.70$ and 0.45, respectively).

5.3. Impact of *NCP* on CO_2 Uptake Over Annual Cycle

[49] Our snapshot observations demonstrate the strong link between *NCP* and CO_2 uptake in the subarctic and transition zone. However, our larger goal is to put these estimates in the context of determining the impact of *NCP* on annual CO_2 uptake in the North Pacific. To do this, we made two box model calculations to examine the seasonal cycle of pCO_2 and *DIC* in our cruise region using a climatological surface pCO_2 data set in boxes of 4° latitude × 5° longitude [*Takahashi et al.*, 2009, section 3.5]. We first examined the seasonal cycle of pCO_2 in a simplified "abiotic" system in which only temperature and gas exchange influence pCO_2 and *CO_2 flux*. Second, we used a simplified *DIC* mass balance approach to compare the annual climatological *CO_2 flux* with the contribution of *NCP* and physical input of *DIC*.

5.3.1. Abiotic pCO_2 Model

[50] A simplified mass balance of DIC in the mixed layer can be written as:

$$\frac{dDIC}{dt} = \frac{1}{h} FCO_{2(in)} + J_{\text{phys}} + J_{\text{ncp}} \tag{4}$$

where $FCO_{2(in)}$ is the sea-air flux of CO_2 ($kCO_2 * k_H(pCO_{2\text{atm}} - pCO_{2\text{SW}})$), with positive $FCO_{2(in)}$ defined as into the ocean (note this is the opposite of the sign convention in equation (3) and our results), h is the mixed layer depth, J_{phys} is the physical input of *DIC* due to advection, diffusion and entrainment (with supply of DIC defined as positive and removal as negative), and J_{ncp} is the export of carbon due to *NCP* (with respiratory source of *DIC* defined as positive and biological uptake of *DIC* as negative). The annual cycle of $FCO_{2(in)}$ is mainly controlled by seasonal changes in surface ocean pCO_2 with a secondary effect of variation in kCO_2 due to seasonal wind speed variation.

[51] To separate the influence of temperature on pCO_2 from the biological and physical effects, we described seasonal changes in pCO_2 in an "abiotic" ocean in which only warming or cooling and air-sea gas exchange influenced seasonal changes in *DIC* and pCO_2. In this case, the *DIC* mass balance simplifies to:

$$\frac{dDIC}{dt} = \frac{1}{h} FCO_{2(in)} = \frac{1}{h} kCO_2 k_H (pCO_{2\text{atm}} - pCO_{2\text{SW}}) \tag{5}$$

[52] We initialized this abiotic model with the 1 March climatological $pCO_{2\text{SW}}$ and *DIC.* We calculated the initial $FCO_{2(in)}$ based on the 1 March climatological $pCO_{2\text{SW}}$, $pCO_{2\text{atm}}$, k_H and kCO_2. We distributed this $FCO_{2(in)}$ over a daily time step and recalculated $dDIC/dt$ and $pCO_{2\text{SW}}$ based on thermodynamic equilibrium (using climatological daily interpolated values of h, alkalinity, $pCO_{2\text{atm}}$, temperature, salinity, k_H and kCO_2; see Methods for details), and repeated the process for each subsequent daily time step. In the region of our study, the mixed layer generally begins to shoal in March, and therefore we assume that any influence of entrainment on *DIC* is negligible until late summer or early fall, when the mixed layer begins to deepen again.

[53] The observed (climatological) pCO_2 peaks in summer in all boxes in our cruise region along 152°W, yielding a summertime CO_2 efflux in all regions (Figure 6). In the abiotic model, however, the estimated summertime increase in pCO_2 (and thus CO_2 efflux) is greater than the observed pCO_2 in all boxes. Biological (J_{ncp}) and physical (J_{phys}; equation (4)) input or removal of *DIC* must be responsible for the difference in annual cycles of the predicted abiotic and observed pCO_2. In spring and summer in the subarctic and transition zone, when the mixed layer is shoaling or stable and wind speeds are low, removal of *DIC* by J_{ncp} is much greater than net removal by J_{phys} [*Ayers and Lozier*, 2012], and is the dominant cause of the observed pCO_2 ($pCO_{2\text{SW}}$) being less than the abiotic pCO_2 ($pCO_{2\text{abio}}$). In the subtropics in spring and summer, based on studies at ALOHA, J_{ncp} is the only term removing *DIC*, because J_{phys} is a net *DIC* source [*Keeling et al.*, 2004; *Quay and Stutsman*, 2003]. In contrast, in fall and winter, when the mixed layer is deepening, addition of *DIC* through positive J_{phys} outweighs removal of *DIC* by J_{ncp} in the subarctic, transition zone and subtropics [*Ayers and Lozier*, 2012;

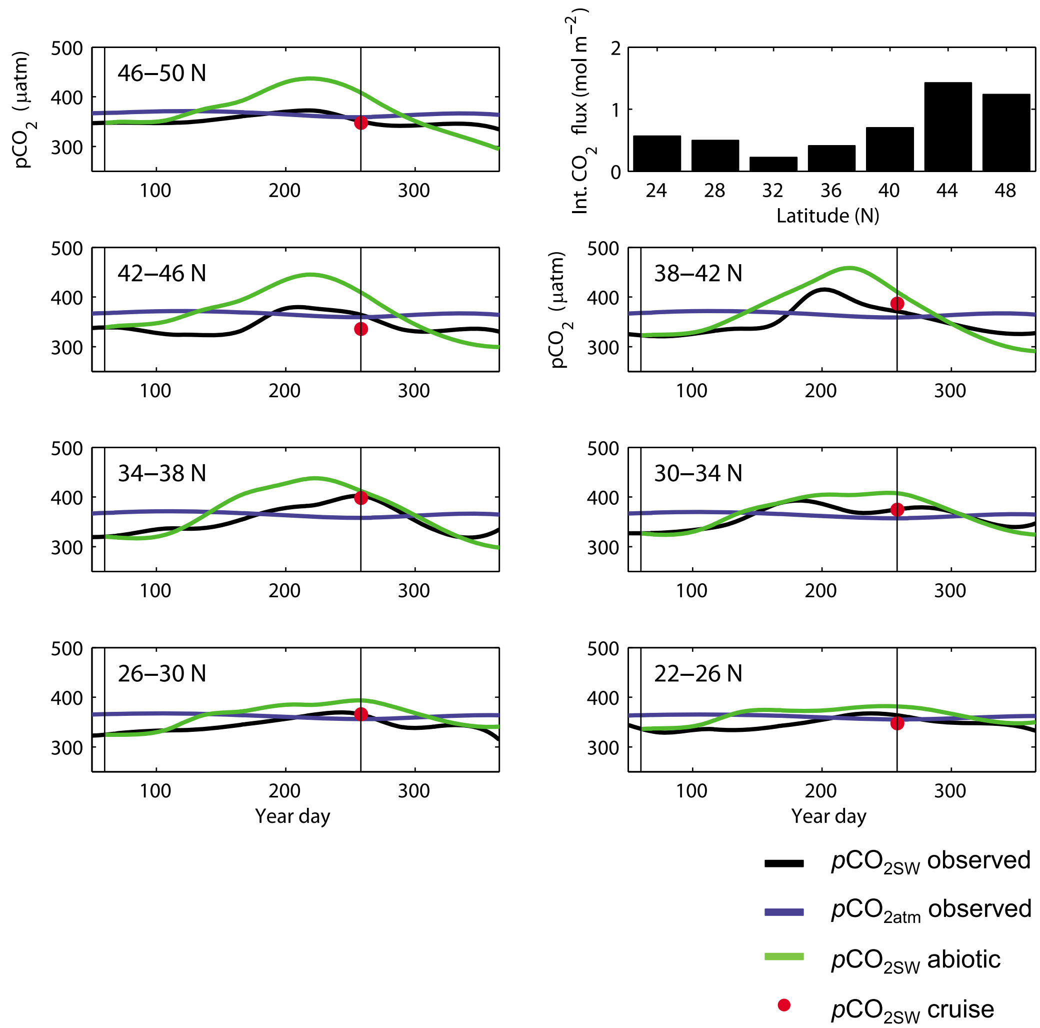

Figure 6. Abiotic model of annual pCO_2 cycle in cruise region along 152°W. Observed (climatological) ocean and atmosphere pCO_2, black and blue lines, respectively. Modeled abiotic pCO_2, green line. Red dot, pCO_2 measured on cruise in this study (September) normalized to year 2000 pCO_2 for consistency with climatological data [*Takahashi et al.*, 2009]. Black vertical lines bound spring-summer period (1 March–15 September). Top right graph, integrated CO_2 flux due to difference between abiotic and observed pCO_2 (for period when abiotic pCO_2 is greater than observed pCO_2 in each box).

Keeling et al., 2004], and causes pCO_{2SW} to be greater than pCO_{2abio}.

[54] We calculated the integrated CO_2 flux resulting from the difference between pCO_{2abio} and pCO_{2SW} by summing daily CO_2 flux = $k_{CO2}\ k_H\ (pCO_{2abio} - pCO_{2SW})$ for the period in each box when pCO_{2abio} is greater than pCO_{2SW}, typically March–September. The trends in this integrated flux along the cruise track largely correspond to the trends in *NCP* and $FCO_{2(in)}$ we observed on our cruise (Figure 6). The integrated flux is greatest in the subarctic (46°N–50°N) and northern transition zone (38°N–46°N), implying high summer drawdown of pCO_2 by *NCP* (assuming J_{phys} is small), in agreement with our cruise observations of high *NCP* and strong coupling of *NCP* and CO_2 uptake in these regions. The integrated flux is lower in the southern transition zone (30°N–38°N) and subtropics (22°N–30°N), in agreement with our cruise observations in these regions of lower *NCP*, CO_2 efflux, and little coupling between *NCP* and $FCO_{2(in)}$. pCO_{2SW} is lower than pCO_{2abio} for the longest interval (>240 days) in the subtropics, as a result of a long growing season, and in the subarctic and northern transition zone (which has both a spring and a fall bloom [*Longhurst*, 2007]).

5.3.2. DIC Mass Balance

[55] We next used a simplified version of the *DIC* mass balance approach of *Lee* [2001] to compare the annual climatological $FCO_{2(in)}$ with the contribution of *NCP*. Rearranging the *DIC* mass balance (equation (4)), the magnitude of *DIC* drawdown plus CO_2 invasion must be the net result of *NCP* plus physical supply:

$$J_{ncp} + J_{phys} = \frac{dDIC}{dt} - \frac{1}{h} FCO_{2(in)}. \tag{6}$$

[56] We again initialized the model with the 1 March value of pCO_2 and climatological *DIC*. We calculated daily $FCO_{2(in)}$ and salinity-normalized $dDIC/dt$ using daily interpolated data described above and solved for $J_{ncp} + J_{phys}$. Initially, we assumed $J_{phys} = 0$ during the well-stratified

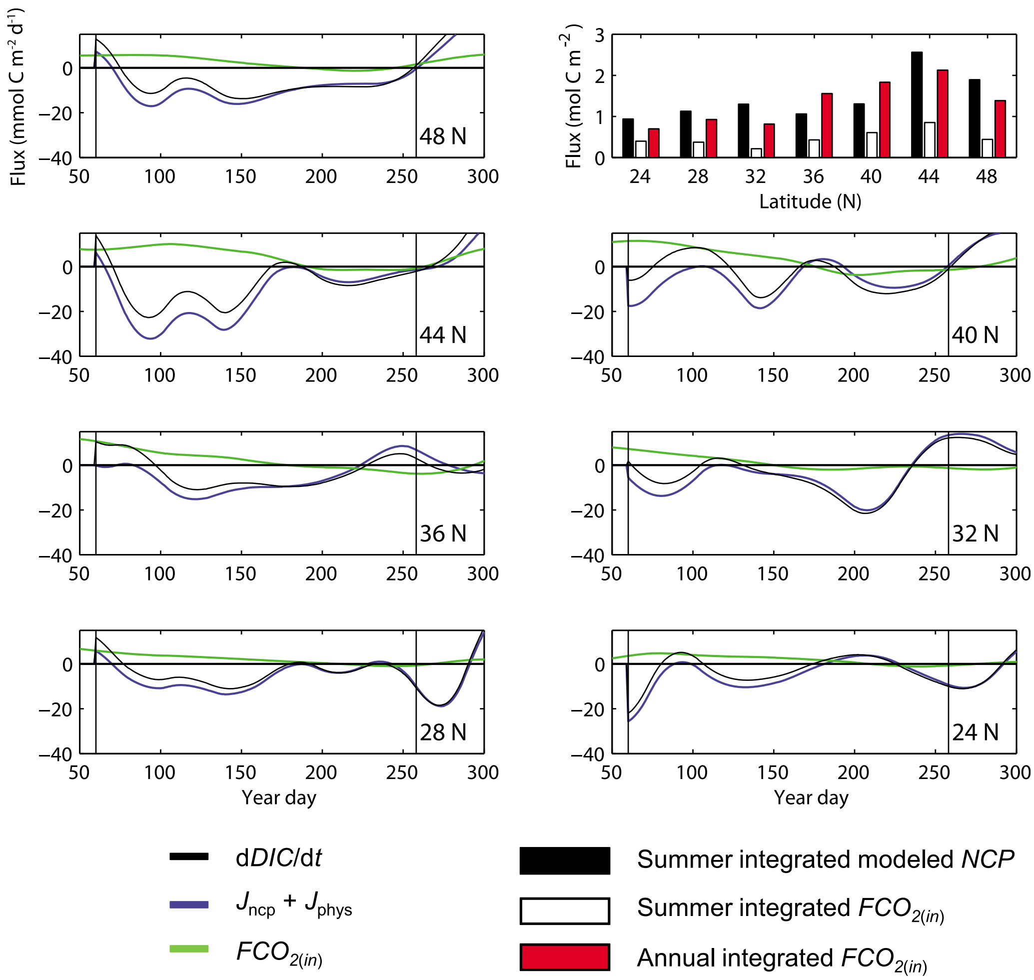

Figure 7. Model of climatological pCO_2 and *DIC* seasonal cycle, distinguishing influence of $FCO_{2(in)}$ and *NCP* plus physical inputs ($J_{ncp} + J_{phys}$) on seasonal changes in DIC (d*DIC*/d*t*). Black vertical lines bound spring-summer period (1 March–15 September) over which summer *NCP* and $FCO_{2(in)}$ (top right) were integrated.

spring-summer season (when observed pCO_2 is less than abiotic pCO_2, typically March–September) to obtain an estimate of J_{ncp}. This would result in an upper-boundary estimate for NCP in the transition zone (where J_{phys} removes a small amount of *DIC* in spring-summer; *Ayers and Lozier*, 2012) and a minimum estimate of *NCP* in the subtropics (where J_{phys} is positive in spring-summer [*Keeling et al.*, 2004]). We integrated this estimate of summer *NCP* by integrating the values of $J_{ncp} + J_{phys}$ for the period 1 March–15 September (Figure 7).

[57] To obtain the observed summertime pCO_2 decrease (if $J_{phys} = 0$) requires mean daily *NCP* in the subarctic and northern transition zone of 10 and 13 mmol C m^{-2} d^{-1}, respectively (Table 3). These values are slightly lower but within the range of uncertainty of previous field estimates for these regions (Table 1). Our cruise-based *NCP* estimate was more than 2× than the model estimate in the subarctic (26 mmol C m^{-2} d^{-1}), likely reflecting the anomalous conditions there during our cruise, and 31% greater in the northern transition zone.

[58] In the southern transition zone and subtropics, modeled summer *NCP* was about half that in the subarctic and northern transition zone, at 5–6 mmol C m^{-2} d^{-1}, similar to our cruise estimates of 5–8 mmol C m^{-2} d^{-1} and within the uncertainty of previous field estimates of *NCP* in these regions (Tables 1 and 3). The ~2× lower summer *NCP* in the subtropics compared to the northern transition zone is similar to the meridional trends in *NCP* estimated from our cruise observations. This suggests that our O_2/Ar-based *NCP* in the transition zone and subtropics during September 2008 may be representative of the climatological *NCP* during the spring-summer growing season. Modeled *NCP* in the subtropics (5 mmol C m^{-2} d^{-1} versus our cruise-based estimate of 8 mmol C m^{-2} d^{-1}) is probably underestimated because physical supply of *DIC* in the subtropics is positive during the summer, as has been shown at ALOHA [*Keeling et al.*, 2004; *Quay and Stutsman*, 2003]. In support of this, the stability ($\Delta\sigma/\Delta z$) in the upper water column in the subtropics and southern transition zone was much less than that in the subarctic during our late summer cruise (Figure 2).

[59] Integrated annual climatological $FCO_{2(in)}$ was similar in magnitude to modeled summer-integrated *NCP* along the cruise track, peaking in the northern transition zone at

Table 3. Results of Model of Climatological pCO_2 and *DIC* Seasonal Cycle

Latitude (N) Along 152°W	Summer-Integrated Modeled *NCP*[a] (mol C m^{-2})	Daily Average Summer Modeled *NCP* (mmol m^{-2} d^{-1})	Summer-Integrated $FCO_{2(in)}$[a] (mol C m^{-2})	Annual-Integrated $FCO_{2(in)}$ (mol C m^{-2} yr^{-1})	Summer-Integrated Modeled *NCP*/Annual-Integrated $FCO_{2(in)}$
46°–50°	1.9	9.5	0.4	1.4	1.4
42°–46°	2.6	13.1	0.9	2.1	1.2
38°–42°	1.3	6.5	0.6	1.8	0.7
34°–38°	1.1	5.5	0.4	1.6	0.7
30°–34°	1.3	6.5	0.2	0.8	1.6
24°–30°	1.1	5.5	0.4	0.9	1.2
22°–24°	0.9	4.5	0.4	0.7	1.3
Subarctic	1.9	9.5	0.4	1.4	1.4
N. Transition	2.0	10.1	0.8	2.0	1.0
S. Transition	1.2	6.0	0.3	1.2	1.2
Subtropics	1.0	5.0	0.4	0.8	1.3

[a]Summer-integrated modeled *NCP* and $FCO_{2(in)}$ are integrated for the period 1 March–15 September. In model, positive $FCO_{2(in)}$ represents influx into ocean. Regions were defined as described in Table 2.

2.0 mol C m^{-2} yr^{-1}, slightly lower in the subarctic and southern transition zone (1.2–1.4 mol C m^{-2} yr^{-1}), and lowest in the subtropics at 0.8 mol C m^{-2} yr^{-1} (Figure 7 and Table 3). On average, the magnitude of summer-integrated *NCP* balances annual-integrated $FCO_{2(in)}$ across the cruise track, with ratios of summer *NCP* to annual $FCO_{2(in)}$ of 0.7–1.4 across all regions (Table 3). Some carbon exported through *NCP* during summer could be remineralized and returned to the mixed layer in winter, as has been observed in the North Atlantic [*Körtzinger et al.*, 2008]; this would lower O_2/Ar-based *NCP* and CO_2 uptake. However, winter mixed layer depths in the NE Pacific are much lower than in the North Atlantic, so the effect may not be as pronounced there.

[60] We conclude that *NCP* exerts a significant control on the high CO_2 uptake in the NE Pacific, with the remainder of annual CO_2 uptake impacted by surface cooling and physical processes. It is difficult to directly estimate the contribution of *NCP* to annual CO_2 uptake, because the response time of CO_2 gas exchange with respect to changes in temperature and DIC is relatively sluggish (~1 year) [*Broecker and Peng*, 1982]. Therefore, *NCP* that takes place in summer likely drives uptake of CO_2 in fall or winter.

6. Conclusions

[61] Mean *NCP* and CO_2 influx along our cruise track were greatest in the subarctic (25.8 ± 4.6 and 4.1 ± 0.9 mmol C m^{-2} d^{-1}, respectively) and the northern transition zone (17.1 ± 4.4 and 2.1 ± 0.5 mmol C m^{-2} d^{-1}, respectively). In the subarctic, our observations of *NCP* were ~2× the mean of previous summer observations, reflecting the influence of an anomalous phytoplankton bloom. In the transition zone, we detected high zonal and meridional variability in *NCP* and *CO_2 flux* at <5-km scales, suggesting the impact of frontal dynamics on biogeochemical fluxes in this region, and the need for observations throughout the year to determine its mean annual state. In the southern transition zone and subtropics, *NCP* (5.4 ± 1.8 and 8.1 ± 2.1 mmol C m^{-2} d^{-1}, respectively) was about 2–3× lower than in the subarctic and northern transition zone, and CO_2 had mean efflux (3.0 ± 0.5 and 0.1 ± 0.0 mmol C m^{-2} d^{-1}, respectively).

[62] *NCP* and CO_2 influx were highly correlated in the subarctic and transition zone with a slope of 2 to 3, indicating the strong coupling between biological uptake and CO_2 influx during summertime in these regions. *NCP* in these regions was also highly correlated with concentrations of microphytoplankton. In contrast, *NCP* and CO_2 influx were not strongly coupled in the subtropics, suggesting that the temperature effect on solubility dominates CO_2 flux during summertime there. In the subtropics, *NCP* was uncorrelated with microphytoplankton and weakly correlated with picophytoplankton, potentially indicating the lower efficiency of a picophytoplankton-dominated biological pump.

[63] Our analysis and modeling of the climatological *DIC* and pCO_2 cycles in the transition zone and subtropics yielded a similar meridional pattern in integrated summertime *NCP* and *CO_2 flux* as we found during our cruise in September 2008. *NCP* in the northern transition zone was ~2–3× that in the southern transition zone and subtropics, suggesting that our snapshot estimates in these regions are representative of the seasonal influence of *NCP* on CO_2 influx. Based on our model of the climatological seasonal *DIC* and pCO_2 cycle in the Northeast Pacific, we conclude that summertime *NCP* is similar in magnitude to the annual atmospheric CO_2 uptake in the NE Pacific, indicating that *NCP* has a significant impact on CO_2 uptake in this region. More continuous observations of the temporal and spatial variability of the biological pump in this region and more sophisticated physical modeling would improve our ability to distinguish the magnitude of the influences of temperature, biological uptake, and physical dynamics in this region of high CO_2 uptake.

[64] **Acknowledgments.** This work was supported by a grant from NSF to P.D.Q., S. Emerson, R.F. and R. Letelier, and a NSF Graduate Research Fellowship (D.L.). We thank Mark Haught, Johnny Stutsman, Fran Janny and David Munro for field and laboratory assistance, and the captain and crew of the R/V *Thomas G. Thompson*. We are grateful to Steven Emerson, David Nicholson and an anonymous reviewer for thoughtful comments that helped us to improve the paper.

References

Ayers, J. M., and M. S. Lozier (2010), Physical controls on the seasonal migration of the North Pacific transition zone chlorophyll front, *J. Geophys. Res.*, *115*, C05001, doi:10.1029/2009JC005596.

Ayers, J. M., and M. S. Lozier (2012), Unraveling dynamical controls on the North Pacific carbon sink, *J. Geophys. Res.*, *117*, C01017, doi:10.1029/2011JC007368.

Benitez-Nelson, C., et al. (2001), A time-series study of particulate matter export in the North Pacific Subtropical Gyre based on ^{234}Th: ^{238}U disequilibrium, *Deep Sea Res., Part I*, *48*, 2595–2611, doi:10.1016/S0967-0637(01)00032-2.

Boyd, P. W., and T. W. Trull (2007), Understanding the export of biogenic particles in oceanic waters: Is there consensus?, *Prog. Oceanogr.*, *72*, 276–312, doi:10.1016/j.pocean.2006.10.007.

Boyd, P. W., et al. (1996), *In vitro* iron enrichment experiments in the NE subarctic Pacific, *Mar. Ecol. Prog. Ser.*, *136*, 179–193, doi:10.3354/meps136179.

Broecker, W. S., and T.-H. Peng (1982), *Tracers in the Sea*, pp. 154–156, Lamont-Doherty Geol. Obs., Palisades, N. Y.

Cassar, N., et al. (2009), Continuous high-frequency dissolved O_2/Ar measurements by equilibrator inlet mass spectrometry, *Anal. Chem.*, *81*, 1855–1864, doi:10.1021/ac802300u.

Cassar, N., et al. (2011), The influence of iron and light on net community production in the subantarctic and polar frontal zones, *Biogeosciences*, *8*, 227–237, doi:10.5194/bg-8-227-2011.

Charette, M. A., S. B. Moran, and J. K. B. Bishop (1999), ^{234}Th as a tracer of particulate organic carbon export in the subarctic northeast Pacific Ocean, *Deep Sea Res., Part II*, *46*, 2833–2861, doi:10.1016/S0967-0645(99)00085-5.

Craig, H., and T. Hayward (1987), Oxygen supersaturation in the ocean: Biological versus physical contributions, *Science*, *235*(4785), 199–202, doi:10.1126/science.235.4785.199.

Denman, K. L., and A. E. Gargett (1995), Biological-physical interactions in the upper ocean: The role of vertical and small scale transport processes, *Annu. Rev. Fluid Mech.*, *27*, 225–256, doi:10.1146/annurev.fl.27.010195.001301.

Emerson, S. (1987), Seasonal oxygen cycles and biological new production in surface waters of the subarctic Pacific ocean, *J. Geophys. Res.*, *92*, 6535–6544, doi:10.1029/JC092iC06p06535.

Emerson, S. R., and J. I. Hedges (2008), *Chemical Oceanography and the Marine Carbon Cycle*, 375 pp., Cambridge Univ. Press, Cambridge, U. K., doi:10.1017/CBO9780511793202

Emerson, S., and C. Stump (2010), Net biological oxygen production in the ocean—II: Remote *in situ* measurements of O_2 and N_2 in subarctic Pacific surface waters, *Deep Sea Res., Part I*, *57*, 1255–1265, doi:10.1016/j.dsr.2010.06.001.

Emerson, S., et al. (1991), O_2, Ar, N_2, and Rn in surface waters of the subarctic ocean: Net biological O_2 production, *Global Biogeochem. Cycles*, *5*, 49–69, doi:10.1029/90GB02656.

Emerson, S., et al. (1995), Chemical tracers of productivity and respiration in the subtropical Pacific Ocean, *J. Geophys. Res.*, *100*, 15,873–15,887, doi:10.1029/95JC01333.

Emerson, S., et al. (1997), Experimental determination of the organic carbon flux from open-ocean surface waters, *Nature*, *389*, 951–954, doi:10.1038/40111.

Emerson, S., C. Stump, and D. Nicholson (2008), Net biological oxygen production in the ocean: Remote in situ measurements of O_2 and N_2 in surface waters, *Global Biogeochem. Cycles*, *22*, GB3023, doi:10.1029/2007GB003095.

Feely, R. A., et al. (1998), A new automated underway system for making high precision pCO$_2$ measurements onboard research ships, *Anal. Chim. Acta*, *377*, 185–191, doi:10.1016/S0003-2670(98)00388-2.

Franks, P. J. S. (1992), Sink or swim: Accumulation of biomass at fronts, *Mar. Ecol. Prog. Ser.*, *82*, 1–12, doi:10.3354/meps082001.

García, H. E., and L. I. Gordon (1992), Oxygen solubility in seawater: Better fitting equations, *Limnol. Oceanogr.*, *37*, 1307–1312, doi:10.4319/lo.1992.37.6.1307.

Guéguen, C., and P. Tortell (2008), High-resolution measurement of Southern Ocean CO_2 and O_2/Ar by membrane inlet mass spectrometry, *Mar. Chem.*, *108*, 184–194, doi:10.1016/j.marchem.2007.11.007.

Hamme, R., and S. Emerson (2004), The solubility of neon, nitrogen and argon in distilled water and seawater, *Deep Sea Res., Part I*, *51*(11), 1517–1528.

Hamme, R., and S. Emerson (2006), Constraining bubble dynamics and mixing with dissolved gases: Implications for productivity measurements by oxygen mass balance, *J. Mar. Res.*, *64*, 73–95, doi:10.1357/002224006776412322.

Hamme, R. C., et al. (2010), Volcanic ash fuels anomalous plankton bloom in subarctic northeast Pacific, *Geophys. Res. Lett.*, *37*, L19604, doi:10.1029/2010GL044629.

Harrison, P. J., P. W. Boyd, D. E. Varela, S. Takeda, A. Shiomoto, and T. Odate (1999), Comparison of factors controlling phytoplankton productivity in the NE and NW subarctic Pacific gyres, *Prog. Oceanogr.*, *43*, 205–234, doi:10.1016/S0079-6611(99)00015-4.

Harrison, P. J., F. A. Whitney, A. Tsuda, H. Saito, and K. Tadokoro (2004), Nutrient and plankton dynamics in the NE and NW gyres of the Subarctic Pacific Ocean, *J. Oceanogr.*, *60*, 93–117, doi:10.1023/B:JOCE.0000038321.57391.2a.

Ho, D. T., C. S. Law, M. J. Smith, P. Schlosser, M. Harvey, and P. Hill (2006), Measurements of air-sea gas exchange at high wind speeds in the Southern Ocean: Implications for global parameterizations, *Geophys. Res. Lett.*, *33*, L16611, doi:10.1029/2006GL026817.

Ho, D. T., R. Wanninkhof, P. Schlosser, D. S. Ullman, D. Hebert, and K. F. Sullivan (2011), Toward a universal relationship between wind speed and gas exchange: Gas transfer velocities measured with ^{3}He/SF$_6$ during the Southern Ocean Gas Exchange Experiment, *J. Geophys. Res.*, *116*, C00F04, doi:10.1029/2010JC006854.

Howard, E., S. Emerson, S. Bushinsky, and C. Stump (2010), The role of net community production in air-sea carbon fluxes at the North Pacific subarctic-subtropical boundary region, *Limnol. Oceanogr.*, *55*(6), 2585–2596, doi:10.4319/lo.2010.55.6.2585.

Intergovernmental Oceanography Commission (1994), *Protocols for the Joint Global Ocean Flux Study (JGOFS) Core Measurements, IOC Manuals and Guides 29*, UNESCO, Paris.

Juranek, L. W. (2007), Assessment of Pacific Ocean organic carbon production and export using measurements of dissolved oxygen isotopes and oxygen/argon gas ratios, PhD diss., School of Oceanogr., Univ. of Washington, Seattle.

Juranek, L. W., and P. D. Quay (2005), In vitro and in situ gross primary and net community production rates in the North Pacific Subtropical Gyre using labeled and natural abundance isotopes of dissolved O_2, *Global Biogeochem. Cycles*, *19*, GB3009, doi:10.1029/2004GB002384.

Juranek, L. W., et al. (2012), Biological production in the NE Pacific and its influence on air-sea CO_2 flux: Evidence from dissolved oxygen isotopes and O_2/Ar, *J. Geophys. Res.*, *117*, C05022, doi:10.1029/2011JC007450.

Kaiser, J., et al. (2005), Marine productivity estimates from continuous O_2/Ar ratio measurements by membrane inlet mass spectrometry, *Geophys. Res. Lett.*, *32*, L19605, doi:10.1029/2005GL023459.

Karl, D. M. (1999), A sea of change: Biogeochemical variability in the North Pacific Subtropical Gyre, *Ecosystems (N. Y.)*, *2*, 181–214, doi:10.1007/s100219900068.

Karl, D., et al. (1997), The role of nitrogen fixation in biogeochemical cycling in the subtropical North Pacific Ocean, *Nature*, *388*, 533–538, doi:10.1038/41474.

Karl, D., R. R. Bidigare, and R. M. Letelier (2001), Long-term changes in plankton community structure and productivity in the North Pacific Subtropical Gyre: The domain shift hypothesis, *Deep Sea Res., Part II*, *48*, 1449–1470, doi:10.1016/S0967-0645(00)00149-1.

Karl, D. M. et al. (2003), Temporal studies of biogeochemical processes determined from ocean time series observations during the JGOFS era, in *Ocean Biogeochemistry: The Role of the Ocean Carbon Cycle in Global Change*, edited by M. J. R. Fasham, pp. 239–267, Springer, Berlin, doi:10.1007/978-3-642-55844-3_11.

Keeling, C. D., H. Brix, and N. Gruber (2004), Seasonal and long-term dynamics of the upper ocean carbon cycle at Station ALOHA near Hawaii, *Global Biogeochem. Cycles*, *18*, GB4006, doi:10.1029/2004GB002227.

Körtzinger, A., U. Send, R. S. Lampitt, S. Hartman, D. W. R. Wallace, J. Karstensen, M. G. Villagarcia, O. Llinás, and M. D. DeGrandpre (2008), The seasonal pCO$_2$ cycle at 49_N/16.5_W in the northeastern Atlantic Ocean and what it tells us about biological productivity, *J. Geophys. Res.*, *113*, C04020, doi:10.1029/2007JC004347.

Langmann, B., K. Zaksek, M. Hort, and S. Duggen (2010), Volcanic ash as fertiliser for the surface ocean, *Atmos. Chem. Phys.*, *10*, 3891–3899, doi:10.5194/acp-10-3891-2010.

Laws, E. A. (1991), Photosynthetic quotients, new production and net community production in the open ocean, *Deep Sea Res.*, *38*, 143–167, doi:10.1016/0198-0149(91)90059-O.

Lee, K. (2001), Global net community production estimated from the annual cycle of surface water total dissolved inorganic carbon, *Limnol. Oceanogr.*, *46*, 1287–1297, doi:10.4319/lo.2001.46.6.1287.

Lee, K., et al. (2006), Global relationships of total alkalinity with salinity and temperature in surface waters of the world's oceans, *Geophys. Res. Lett.*, *33*, L19605, doi:10.1029/2006GL027207.

Leonard, C., R. R. Bidigare, M. P. Seki, and J. J. Polovina (2001), Interannual mesoscale physical and biological variability in the North Pacific Central Gyre, *Prog. Oceanogr.*, *49*, 227–244, doi:10.1016/S0079-6611(01)00024-6.

Lewis, E., and D. W. R. Wallace (1998), *Program developed for CO_2 system calculations, ORNL/CDIAC-105*, 21 pp., Carbon Dioxide Inf.

Anal. Cent., Oak Ridge Natl. Lab, Oak Ridge, Tenn., doi:10.2172/639712.
Longhurst, A. (2007), *Ecological Geography of the Sea*, Acad. Press, San Diego, Calif.
Mann, K. H., and J. R. N. Lazier (2006), *Dynamics of Marine Systems: Biological-Physical Interactions in the Oceans*, 3rd ed., Blackwell, Malden, Mass.
Monterey, G., and S. Levitus (1997), *Seasonal Variability of Mixed Layer Depth for the World Ocean. NOAA Atlas NESDIS 14*, 96 pp., U.S. Gov. Print. Off., Washington, D. C.
Nemcek, N., D. Ianson, and P. D. Tortell (2008), A high-resolution survey of DMS, CO2, and O2/Ar distributions in productive coastal waters, *Global Biogeochem. Cycles*, *22*, GB2009, doi:10.1029/2006GB002879.
Nightingale, P. D., G. Malin, C. S. Law, A. J. Watson, P. S. Liss, M. I. Liddicoat, J. Boutin, and R. C. Upstill-Goddard (2000), *In situ* evaluation of air-sea exchange parameterizations using novel conservative and volatile tracers, *Global Biogeochem. Cycles*, *14*(1), 373–387, doi:10.1029/1999GB900091.
Olson, D. B., et al. (1994), Life on the edge: Marine life and fronts, *Oceanography*, *7*(2), 52–60.
Pierrot, D., et al. (2009), Recommendations for autonomous underway pCO_2 measuring systems and data-reduction routines, *Deep Sea Res., Part II*, *56*, 512–522, doi:10.1016/j.dsr2.2008.12.005.
Polovina, J. J., et al. (2001), The transition zone chlorophyll front, a dynamic global feature defining migration and forage habitat for marine resources, *Prog. Oceanogr.*, *49*, 469–483, doi:10.1016/S0079-6611(01)00036-2.
Quay, P. D., and J. Stutsman (2003), Surface layer carbon budget for the subtropical N. Pacific: $\delta^{13}C$ constraints at station ALOHA, *Deep Sea Res., Part I*, *50*, 1045–1061, doi:10.1016/S0967-0637(03)00116-X.
Quay, P. D., J. Stutsman, R. A. Feely, and L. W. Juranek (2009), Net community production rates across the subtropical and equatorial Pacific Ocean estimated from air-sea $\delta^{13}C$ disequilibrium, *Global Biogeochem. Cycles*, *23*, GB2006, doi:10.1029/2008GB003193.
Quay, P. D., C. Peacock, K. Björkman, and D. M. Karl (2010), Measuring primary production rates in the ocean: Enigmatic results between incubation and non-incubation methods at Station ALOHA, *Global Biogeochem. Cycles*, *24*, GB3014, doi:10.1029/2009GB003665.
Reuer, M. K., et al. (2007), New estimates of Southern Ocean biological production rates from O_2/Ar ratios and the triple isotope composition of O_2, *Deep Sea Res., Part I*, *54*, 951–974, doi:10.1016/j.dsr.2007.02.007.
Roden, G. I. (1991), Subarctic-subtropical transition zone of the North Pacific: Large-scale aspects and mesoscale structure, in *Biology, oceanography, and fisheries of the North Pacific Transition Zone and Subarctic Frontal Zone*, NOAA Tech. Rep. NMFS 105, edited by J. A. Wetherall et al., pp. 1–38, Natl. Mar. Fish. Serv, Silver Spring, Md.
Schlitzer, R. (2000), Applying the adjoint method for global biogeochemical modeling: Export of particulate organic matter in the world ocean, in *Inverse Methods in Global Biogeochemical Cycles*, *Geophys. Monogr. Ser.*, edited by P. Raynor et al., pp. 107–124, AGU, Washington, D. C., doi:10.1029/GM114p0107.
Schlitzer, R. (2004), Export production in the equatorial and north Pacific derived from dissolved oxygen, nutrient and carbon data, *J. Oceanogr.*, *60*, 53–62, doi:10.1023/B:JOCE.0000038318.38916.e6.
Sherr, E. B., B. F. Sherr, and P. A. Wheeler (2005), Distribution of coccoid cyanobacteria and small eukaryotic phytoplankton in the upwelling ecosystem off the Oregon coast during 2001 and 2002, *Deep Sea Res., Part II*, *52*, 317–330, doi:10.1016/j.dsr2.2004.09.020.
Stanley, R. H. R., J. B. Kirkpatrick, N. Cassar, B. A. Barnett, and M. B. Bender (2010), Net community production and gross primary production rates in the western equatorial Pacific, *Global Biogeochem. Cycles*, *24*, GB4001, doi:10.1029/2009GB003651.
Strass, V. H. (1992), Chlorophyll patchiness caused by mesoscale upwelling at fronts, *Deep Sea Res.*, *39*(1), 75–96, doi:10.1016/0198-0149(92)90021-K.
Strickland, J. D. H., and T. R. Parsons (1972), *A Practical Handbook of Seawater Analysis*, 2nd ed., Fish. Res. Board of Canada, Ottawa.
Stumm, W., and J. J. Morgan (1996), *Aquatic Chemistry: Chemical Equilibria and Rates in Neutral Waters*, 3rd ed., Wiley, New York.
Sweeney, C., E. Gloor, A. R. Jacobson, R. M. Key, G. McKinley, J. L. Sarmiento, and R. Wanninkhof (2007), Constraining global air-sea gas exchange for CO_2 with recent bomb 14C measurements, *Global Biogeochem. Cycles*, *21*, GB2015, doi:10.1029/2006GB002784.
Takahashi, T., et al. (2002), Global sea-air CO_2 flux based on climatological surface ocean pCO_2, and seasonal biological and temperature effects, *Deep Sea Res., Part II*, *49*, 1601–1622, doi:10.1016/S0967-0645(02)00003-6.
Takahashi, T., et al. (2009), Climatological mean and decadal change in surface ocean pCO_2, and net sea–air CO_2 flux over the global oceans, *Deep Sea Res., Part II*, *56*, 554–577, doi:10.1016/j.dsr2.2008.12.009.
Tortell, P. D. (2005), Dissolved gas measurements in oceanic waters made by membrane inlet mass spectrometry, *Limnol. Oceanogr. Methods*, *3*, 24–37, doi:10.4319/lom.2005.3.24.
Wanninkhof, R. (1992), Relationship between wind speed and gas exchange over the ocean, *J. Geophys. Res.*, *97*, 7373–7382, doi:10.1029/92JC00188.
Wheeler, P. A. (1993), New production in the subarctic Pacific Ocean: Net changes in nitrate concentrations, rates of nitrate assimilation and accumulation of particulate nitrogen, *Prog. Oceanogr.*, *32*, 137–161, doi:10.1016/0079-6611(93)90011-2.
Wilson, C. (2003), Late summer chlorophyll blooms in the oligotrophic North Pacific Subtropical Gyre, *Geophys. Res. Lett.*, *30*(18), 1942, doi:10.1029/2003GL017770.
Wilson, C., et al. (2008), Biological and physical forcings of late summer chlorophyll blooms at 30°N in the oligotrophic Pacific, *J. Mar. Syst.*, *69*, 164–176, doi:10.1016/j.jmarsys.2005.09.018.
Wong, C. S., et al. (2002a), Time-series study of the biogeochemistry of the North East subarctic Pacific: Reconciliation of the Corg/N remineralization and uptake ratios with the Redfield ratios, *Deep Sea Res., Part II*, *49*, 5717–5738, doi:10.1016/S0967-0645(02)00211-4.
Wong, C. S., et al. (2002b), Seasonal cycles of nutrients and dissolved inorganic carbon at high and mid latitudes in the North Pacific Ocean during the Skaugran cruises: Determination of new production and nutrient uptake ratios, *Deep Sea Res., Part II*, *49*, 5317–5338, doi:10.1016/S0967-0645(02)00193-5.
Yuan, X., and L. D. Talley (1996), Characteristics of frontal structure from climatological data and synoptic surveys, *J. Geophys. Res.*, *101*, 16,491–16,508, doi:10.1029/96JC01249.